

# A Modelling Approach to Monitor Friction within Electromechanical Actuator Ballscrews using Motor Current

Yameen M. Hussain<sup>1</sup>, Stephen Burrow<sup>2</sup>, Leigh Henson<sup>3</sup>, Patrick Keogh<sup>4</sup>

<sup>1,2</sup>*University of Bristol, Bristol, BS8 1TR, United Kingdom  
yameen.hussain@bristol.ac.uk  
Stephen.Burrow@bristol.ac.uk*

<sup>3</sup>*Stirling Dynamics Ltd, Bristol, BS8 4HG, United Kingdom  
Leigh.Henson@stirling-dynamics.com*

<sup>4</sup>*University of Bath, Bath, BA2 7AY, United Kingdom  
p.s.keogh@bath.ac.uk*

## ABSTRACT

A modelling approach to monitor ballscrew friction within Electromechanical Actuators (EMA) using motor current is presented along with subsequent fault diagnostics using classification of simulated data for healthy, degrading and faulty states. An approach was used where a baseline linear EMA system was modelled to a high level of detail. The modelling involved emphasis on the Permanent Magnet Synchronous Motor (PMSM) where a greater understanding of the drivetrain could be achieved. The PMSM was modelled using ‘dq axis’ transformation theory. The mechanical elements of the EMA were also modelled to include non-linear characteristics. Interaction between the ball and nut, and ball and screw are considered the main source of friction within the ballscrew, hence sliding velocities in these contact areas were used to calculate velocity dependent friction using the Stribeck friction model. Contact angles between ball and nut, and ball and screw, and mechanical efficiencies were varied to analyse the effect on the torque producing current for healthy, degrading and faulty conditions. The simulated data was trained for each condition for classification using a k-Nearest Neighbour (k-NN) algorithm. The first part of the analysis revealed that ballscrew degradation should be detectable using motor current by monitoring changes to the torque producing q-axis current for each failure state in the ballscrew damage model. External load disturbances were also modelled since they could cause fluctuations to the q-axis currents thus making it difficult to isolate deteriorations to the ballscrew. The

simulated datasets were processed for classification as training data using the k-NN algorithm where a classification accuracy of ~74% was achieved. Overall, the in-depth modelling of the EMA system presented a comprehensive approach to monitoring ballscrew friction through use of motor current analysis from different test cases. It is proposed that employing a hybrid approach (combination of model based and data driven techniques) to fault diagnostics can further improve the classification accuracy.

**Keywords—** *Prognostics; Health Monitoring; Aerospace; Electromechanical Actuators; Ballscrew; Fault Classification*

## 1. INTRODUCTION

There is a move towards ‘more electric’ aircraft within the aerospace industry, which has prompted aircraft manufacturers to consider replacing traditional hydromechanical solutions for EMAs in actuation systems to fulfil the need for better maintainability, precision control and offer a weight saving advantage (Hoffman et al. 1985). EMAs are becoming prominent in safety critical applications of next generation fly-by-wire aircraft (Balaban et al. 2011). This is true for applications such as primary flight control systems and landing gear systems. The absence of reliable fail-safe mechanisms and adequate redundancy to mitigate the single point of failure (ballscrew jamming) has made it challenging to introduce EMAs in such safety critical systems (Balaban et al. 2009). It is widely understood that Prognostics and Health Monitoring (PHM) of such systems could mitigate ballscrew jamming, however, research in this area has revealed that the issue is complex for PHM designers due to the limitations in sensing. Aircraft manufacturers are reluctant to add more sensors due to added weight implications (Donald et al. 2004) and reliability and so PHM

Yameen M. Hussain et al. This is an open-access article distributed under the terms of the Creative Commons Attribution 4.0 International License, which permits unrestricted use, distribution, and reproduction in any medium, provided the original author and source are credited.

designers have to rely on motor current alone to detect the onset of ballscrew jamming. Therefore, the purpose of this paper is to demonstrate a means to monitor friction build up within the ballscrew using motor current for feature classification and fault diagnostics.

### 1.1. Background

As mentioned, one of the major concerns has been EMA jamming which is a single point of failure. The mitigation of this failure mode could lead to a fully compliant and airworthy implementation for aircraft safety-critical systems. In view of this issue, significant research has been conducted by PHM designers in an attempt to detect and predict the onset of ballscrew jamming. EMAs consist of a motor, gearing and a ballscrew to provide incremental linear motion powered by the motor. Figure 1 shows a schematic of a typical EMA system.

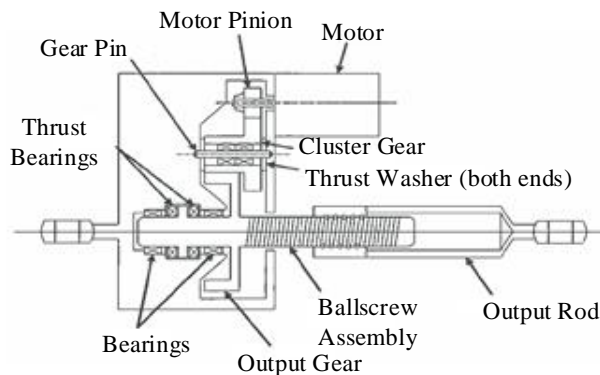


Figure 1. EMA System (Bodden et al. 2007).

It is known that EMAs can fail in many ways (Bennett et al. 2010) with significant research conducted to achieve a fault tolerant EMA system to mitigate single points of failure. Much of this research has been centred around achieving fault tolerant designs for motor related failures for general applications. Motor rotor failures and short circuits are classed as one of the most severe types of failure as they can lead to a complete loss of operation at a system level. Within aerospace, however, there is adequate motor redundancy and therefore such failures would not inhibit operation of an EMA system (Bennett et al. 2010).

Mitigating ballscrew jamming in aerospace is given high importance as failure can lead to complete loss of operation of the landing gear extension/retraction or flight control system mechanism. The build up of friction and wear is identified as a precursor for ballscrew jamming (Lee et al. 2015). As has been established from past data-driven based research, a reliable combination of sensing to monitor vibration, motor current, temperature and loads can help monitor the condition of an EMA (Isturiz et al. 2012). However, there is no guarantee that state of the art sensing would be able to isolate the occurrence of a particular failure

mode such as EMA ballscrew jamming. There are further limitations in which maintenance engineers only have motor current and speed/position data for fault detection in real applications. Therefore, diagnostics engineers must design a robust PHM algorithm to detect the onset of EMA jamming with these limitations in mind.

Research in this area has considered many strategies and technologies using PHM. Whilst research has been conducted in terms of applying PHM to EMAs, an optimum solution to mitigating jamming is still sought. Isolation of jamming failures by utilising test rig analysis for seeded failure tests and run-to-failure data has been undertaken by Balaban et al. (2009). This includes work where jamming faults were injected into a custom made EMA test stand. The results showed good agreement with developed thermal and mechanical models. The issue, however, is the abrupt nature in which the failure occurs making it difficult to detect the onset of this failure. Bodden et al. (2007) also conducted seeded failure testing on an EMA test stand. The methodology evaluated actuator efficiency by monitoring overall power output against input. The analysis revealed that it was difficult to ascertain the origin of the fault at a local level.

Therefore, the main challenges in employing a test stand data driven analysis include: not being able to simulate naturally occurring faults as well as isolating a particular fault within the drivetrain.

### 1.2. Aims and Objectives

This paper aims to provide an advancement to assessing ballscrew degradation through motor current signals. A high fidelity model of the EMA system is used to establish a link between motor current and ballscrew friction.

The primary objectives of this paper are as follows:

1. Determine whether it is possible to detect the presence of friction within the ballscrew using motor current alone through a modelling based approach.
2. Train and classify simulated datasets using the k-NN algorithm to evaluate model robustness for other test cases.

## 2. METHODOLOGY

The first part of the methodology consists of a series of procedures and equations for EMA modelling to develop an enhanced understanding of the baseline linear EMA system.

The second part of the methodology describes how motor current shall be used to aid fault detection and diagnostics of the ballscrew. This is followed by a description of the test

cases and conditions to be simulated for healthy, degrading and failure states of the ballscrew.

The final part of the methodology describes the data analysis technique to be applied to the simulated data for each test case towards data training for classification.

## 2.1. EMA Modelling

The system being modelled is a baseline linear EMA system. The modelling was conducted using Matlab/Simulink where the key components consisted of the motor controller, the PMSM and the ballscrew. Figure 2 shows a high level view of the EMA system being modelled for speed & current control.

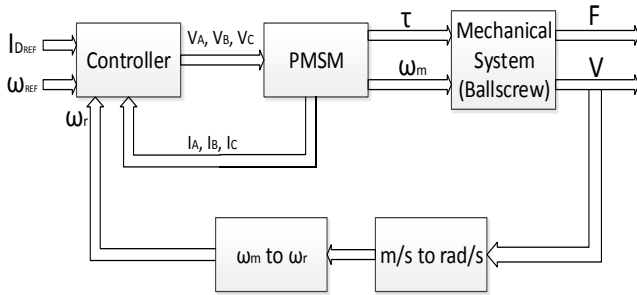


Figure 2. EMA Block Diagram.

PMSM's use permanent magnets rather than windings in the rotor. Electronic excitation control with integrated power inverter and rectifier, sensor, and inverter electronics are required for practical operation (Vas, 1996). The PMSM was modelled using 'dq-axis transformation' theory which involves Park's transform. Park's transform reduces 3-phase AC quantities ( $I_A$ ,  $I_B$ ,  $I_C$ ) to DC quantities ( $I_D$ ,  $I_Q$ ) (Park, 1929). The transform to DC quantities reduces the complexity of the system and therefore more understanding of the drivetrain system can be achieved by modelling the PMSM in this way. Figure 3 shows the equivalent electrical circuit for the PMSM.

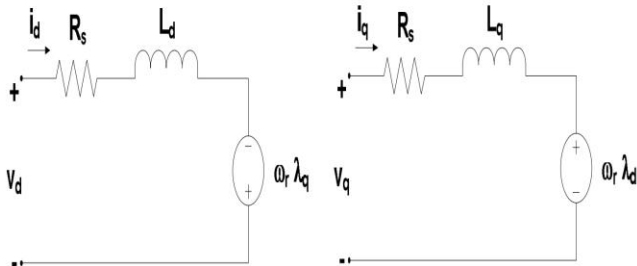


Figure 3. PMSM Equivalent Electric Circuit in Rotating Reference Frame (DQ).

The transformation converts vectors in the 3-phase reference frame to 2-phase and then a rotating 2-phase reference frame as shown in Figure 4.

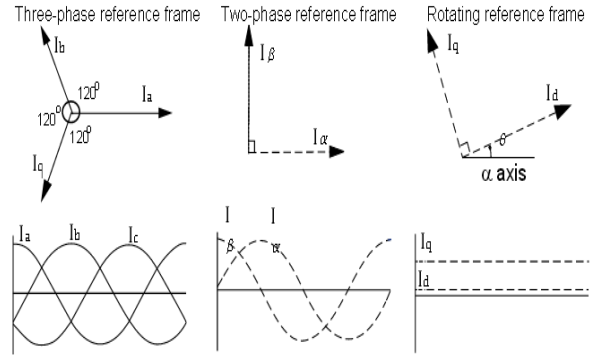


Figure 4. Reference Frames.

This enables simplified analysis of these DC quantities before performing the inverse transform to the 3-phase results. This will provide in-depth motor understanding for condition monitoring and fault detection.

The PMSM was modelled in accordance to a specification with parameters listed in Table 1.

Table 1. PMSM Parameters.

Parameter	Value
Resistance, $R_s$	1.1 ohm
Speed	3000 RPM
Motor Voltage Constant, $K_e$	98 V/Krpm
Motor Torque Constant, $K_t$	1.6 Nm/A
Peak Torque, $\tau$	45.9 Nm
Peak Current, $I$	28.7 A
Poles, $p$	6
Inductance on q-axis, $L_q$	12 mH
Inductance on d-axis, $L_d$	7.4 mH
Motor Inertia, $J$	0.138 kg.m <sup>2</sup>

The electrical and mechanical elements of the PMSM were modelled within the PMSM block shown in Figure 2. Firstly, the 3-phase supply voltages were converted to 2-phase quantities using Park's transform:

$$\begin{bmatrix} V_d \\ V_q \\ V_0 \end{bmatrix} = \frac{2}{3} \begin{bmatrix} \cos\theta & \cos\left(\theta - \frac{2\pi}{3}\right) & \cos\left(\theta + \frac{2\pi}{3}\right) \\ -\sin\theta & -\sin\left(\theta - \frac{2\pi}{3}\right) & -\sin\left(\theta + \frac{2\pi}{3}\right) \\ \frac{1}{2} & \frac{1}{2} & \frac{1}{2} \end{bmatrix} \begin{bmatrix} V_a \\ V_b \\ V_c \end{bmatrix} \quad (1)$$

The PMSM electrical model consists of the stator resistance, inductances (d and q axes), number of poles as well as the flux induced by the rotor permanent magnets in the stator phases to get the  $I_q$  and  $I_d$  currents:

$$V_d = R_s I_d + p \lambda_d - \omega_r \lambda_q \quad (2)$$

$$V_q = R_s I_q + p \lambda_q + \omega_r \lambda_d \quad (3)$$

Where

$$\lambda_d = L_d I_d + \lambda_{af} \quad (4)$$

and

$$\lambda_q = L_q I_q \quad (5)$$

The electromagnetic torque of the PMSM is derived from:

$$T_e = \frac{3p}{4} (\lambda_d I_q - \lambda_q I_d) = \frac{3p}{4} (\lambda_{af} I_q + (L_d - L_q) I_d I_q) \quad (6)$$

The mechanical subsystem of the PMSM model to calculate mechanical torque and rotor mechanical speed is given by

$$T_e = T_L + B \omega_m + J \frac{d\omega_m}{dt} \quad (7)$$

Equation (7) can be rearranged for rotor mechanical speed:

$$\omega_m = \int \left( \frac{T_e - T_L - B \omega_m}{J} \right) dt \quad (8)$$

whereby the relationship between the electrical speed ( $\omega_r$ ) and the rotor mechanical speed ( $\omega_m$ ) is given by

$$\omega_m = \omega_r \left( \frac{2}{p} \right) \quad (9)$$

Given the modelled PMSM electrical and mechanical properties, the d and q axis currents are transformed back into 3-phase quantities and subsequently fed back in to the PMSM controller block (as shown in Figure 2). The inverse Park transform was used to return the 3-phase currents:

$$\begin{bmatrix} I_a \\ I_b \\ I_c \end{bmatrix} = \begin{bmatrix} \cos \theta & -\sin \theta & 1 \\ \cos \left( \theta - \frac{2\pi}{3} \right) & -\sin \left( \theta - \frac{2\pi}{3} \right) & 1 \\ \cos \left( \theta + \frac{2\pi}{3} \right) & -\sin \left( \theta + \frac{2\pi}{3} \right) & 1 \end{bmatrix} \begin{bmatrix} I_d \\ I_q \\ I_0 \end{bmatrix} \quad (10)$$

The PMSM controller is modelled for speed and torque control. This enables real time control of torque variation demand, mechanical speed and regulation of the phase currents, which ultimately reduces the occurrence of current spikes during transient operation. Figure 5 shows a block diagram of the PMSM speed and current control system.

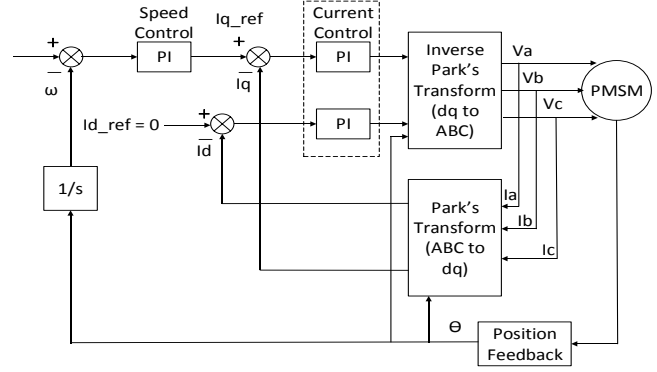


Figure 5. PMSM Speed and Current Controller.

The ballscrew is modelled by taking the generated mechanical torque and rotor speed values and converting them in to end loads and linear speeds. The ballscrew specification is presented in Table 2.

Table 2. Ballscrew Parameters.

Parameter	Value
Lead, L	5
Length, l	300 mm
Screw Diameter, $D_s$	20 mm
Ball Diameter, D	5 mm
Ballscrew Helical Angle, $\alpha$	55°
Screw Pitch Diameter, $d_s$	18 mm
Nut Inner Diameter, $d_n$	20.8 mm

The ballscrew linear velocity is given by

$$V = \frac{\omega_m L}{2\pi} \quad (11)$$

The ballscrew end load (F) is given by

$$F = \frac{2T_e \pi \eta}{L} \quad (12)$$

Friction is mostly prevalent between the ball and screw thread (Vahid-Araghi and Golnaraghi, 2011). Friction also occurs between the ball and nut and therefore the analysis focuses on these areas of interaction within the ballscrew. A kinematic analysis of this region was required in order to understand these contact areas in more detail and to evaluate friction as a function of sliding velocity.

A thorough mathematical model of ballscrew kinematics has been developed by Wei et al. (2004) therefore this was utilised partially for this segment of the research.

Firstly, the relative velocities between ball and screw,  $V_{BS}$  and ball and nut  $V_{BN}$ , needed to be factored in. Relative speeds of these regions are critical for this study as they largely dictate the magnitude of instability when the ballscrew experiences

a fault (Jiang et al. 2010). The corresponding relative angular velocities are given by

$$\omega_{BS} = \frac{V_{BS}}{0.5(d_s - D)} \quad (13)$$

$$\omega_{BN} = \frac{V_{BN}}{0.5d_n} \quad (14)$$

Information regarding the rotor mechanical speed, ( $\omega_m$ ) is known therefore the angular velocities were calculated using a detailed kinematic analysis. Wei et al. (2004) determined the relationship between the angular velocities,  $\omega_{BS}$  and  $\omega_{BN}$  as

$$\frac{\omega_{BS}}{\omega_{BN}} = \frac{(1 + \delta \cos \alpha_n)(\cos \alpha_s + \tan \beta \sin \alpha_s)}{(1 - \delta \cos \alpha_s)(\cos \alpha_n + \tan \beta \sin \alpha_n)} \quad (15)$$

$\beta$  is the lead angle and  $\delta$  is a relationship between ball diameter and screw pitch given by

$$\delta = \frac{D}{d_s} \quad (16)$$

The contact angles (between ball and nut,  $\alpha_n$ , and ball and screw,  $\alpha_s$ ) are depicted in Figure 6.

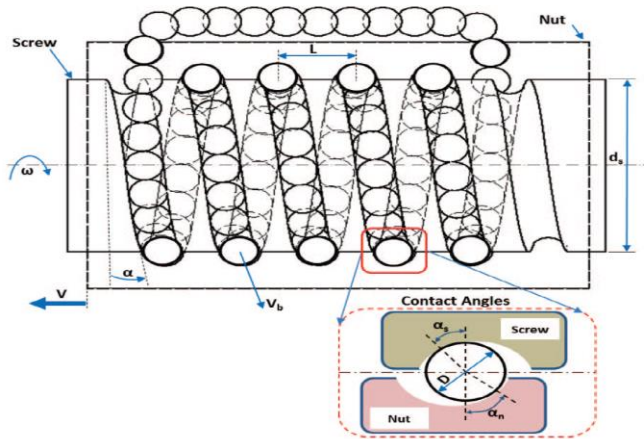


Figure 6. Ballscrew Kinematics (Ismail et al. 2016).

In order to calculate the relative angular velocities ( $\omega_{BS}$  and  $\omega_{BN}$ ), ball linear velocity,  $V_b$  needs to be ascertained. Assuming the relative slip speed between ball and nut is negligible,  $V_b$  can be calculated as follows (Song et al. 2005):

$$V_b = \frac{\omega_m(D_s - D \sin \alpha) \cos \beta}{2} \quad (17)$$

Where the lead angle,  $\beta$  is determined from

$$\tan \beta = \frac{L}{\pi D} \quad (18)$$

Given equation (17), the corresponding ball angular velocity,  $\omega_b$  is given by:

$$\omega_b = \frac{V_b}{0.5d_s} \quad (19)$$

The relative angular velocity between ball and screw,  $\omega_{BS}$  depends on ball angular velocity,  $\omega_b$  and ballscrew angular velocity,  $\omega_m$  (Wei and Lin, 2004), hence

$$\omega_{BS} = (\omega_m - \omega_b) \cos \alpha \quad (20)$$

The relative angular velocity between ball and nut,  $\omega_{BN}$  depends only on the ball angular velocity,  $\omega_b$  (Wei and Lin, 2004) therefore:

$$\omega_{BN} = -\omega_b \cos \alpha \quad (21)$$

Given that  $\omega_{BS}$  and  $\omega_{BN}$  can now be calculated as a function of ball angular velocity,  $\omega_b$ , equations (20) and (21) can be substituted into equation (15) and rearranged to obtain

$$\omega_{BS} = \omega_{BN} \frac{(1 + \delta \cos \alpha_n)(\cos \alpha_s + \tan \beta \sin \alpha_s)}{(1 - \delta \cos \alpha_s)(\cos \alpha_n + \tan \beta \sin \alpha_n)} \quad (22)$$

$$\omega_{BN} = \omega_{BS} \frac{(1 - \delta \cos \alpha_s)(\cos \alpha_n + \tan \beta \sin \alpha_n)}{(1 + \delta \cos \alpha_n)(\cos \alpha_s + \tan \beta \sin \alpha_s)} \quad (23)$$

The next step was to formulate a velocity dependent coefficient of friction model given the relative velocities between the ball and nut, and ball and screw. The Stribeck friction model (Bowden and Tabor, 1950) was used to evaluate friction between the interacting surfaces in the ballscrew. This was used previously by Vahid-Araghi and Golnaraghi (2011) for a lead screw drive system. The velocity dependent coefficient of friction is generally composed of:

- Coulomb friction,  $F_c$  – Constant friction force opposing motion.
- Viscous friction,  $F_v$  - Friction force proportional to the sliding velocity.
- Stribeck friction,  $F_s$  – Occurs at low sliding velocities and contains Coulomb and Viscous friction components as shown in Figure 7.

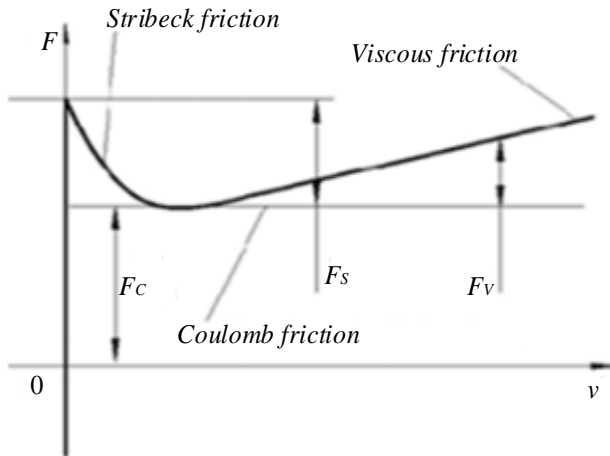


Figure 7. Velocity Dependent Coefficient of Friction.

$$F = F_c + F_s \left( e^{-\frac{|v_s|}{v_0}} - 1 \right) + F_v |v_s| \quad (24)$$

where  $v_s$  is the sliding velocity between interacting surfaces. This was treated as the relative speed between ball and nut, and ball and screw as described earlier in this section.  $v_0$  controls the velocity range of the Stribeck effect.

The overall friction is then added into the end load model, which is then converted back into mechanical torque. Using the motor torque constant,  $K_t$ ,  $I_q$  current values were calculated to aid the friction detection analysis within the ballscrew using motor current.

The procedure to calculate  $I_q$  current as a result of different motor demand speeds and variations in friction and mechanical efficiency can be summarised in the following steps:

- i Set motor demand speed, mechanical system efficiency and contact angles between ball and nut, and ball and screw.
- ii Calculate generated friction force after running simulation.
- iii Add friction force to overall EMA end load.
- iv Calculate corresponding torque due to additional loads.
- v Using the motor torque constant, calculate updated  $I_q$  current.

## 2.2. Test Cases and Conditions

Using the model described in Section 2.1, a series of simulations were evaluated using different variables that include contact angles between ball and nut, and ball and

screw, mechanical efficiencies and demand speeds. A typical landing gear extension/retraction cycle for a Boeing 757 is required to complete in ~20 seconds (Boeing, 1994) therefore a cycle time of 20 seconds was used for this analysis.

One of the primary objectives of this paper is to identify the onset of ballscrew jamming using a model based approach therefore test cases for simulation were created with respect to 3 states of health: Healthy, Degrading and Faulty.

### Healthy State

Contact angles between ball and nut, and ball and screw typically range between 38-40° (Ninomiya and Miyaguchi, 1998). Therefore, these values were used to represent a healthy condition for the ballscrew and nut.

Mechanical efficiency is the measure of effectiveness of the EMA's input power over the output, which produces the end force and motion. Industry standard values were used for ballscrew mechanical efficiency which is generally in the region of ~80-90% for healthy states (McNier, 2016).

### Degrading State

Degrading states are conditions where the EMA is operable, but exhibits deteriorations in performance due to wear and build up of friction. Ballscrew and nut contact angles can vary upto 8% through deterioration, misalignment cases or incorrect selection (Xu et al. 2014). Therefore such instances were simulated by inducing variation in the contact angles of up to 8%.

Ballscrew mechanical efficiencies are also significantly lower therefore values between 35-65% were used in this state. Mechanical efficiencies of 70-80% were also tested for such cases of variation in contact angles.

### Faulty State

The analysis is focused on one type of EMA failure mode, ballscrew jamming. The onset of jamming is of interest and so lower mechanical efficiency values (15-35%) were modelled to evaluate the effect on motor current.

The relative velocities (between ball and nut, and ball and screw) were set to zero to represent the jamming condition.

Table 3 summarises the test cases and conditions that were simulated.

Table 3. Test Cases and Conditions Summary.

State	Ball – Nut and Ball – Screw Angle of Contact (degrees)	Mechanical Efficiency (%)
Healthy	38-40	70-80
Degradng	35-43	70-80
		35-65
Faulted	Relative velocity set close to 0 (onset of jamming)	15-35

Simulations for each of the test cases for the different states were run for different motor command speeds: 500, 1500 and 3000 RPM.

In addition, external disturbances can occur in an EMA application, e.g. gust and aeroloads for a landing gear actuation system, which can induce uncertainty in ascertaining the true state of health. Therefore, instantaneous loads through a single cycle were modelled to replicate these disturbances. These loads were simulated in two ways:

- Load factor (x1.2) applied at a constant level throughout cycle.
- Pulse signals induced to represent load impulses during the cycle.

Following the simulations, mean  $I_q$  motor currents were generated for post analysis and training for classification. A total of 667  $I_q$  current datasets were generated which included different contact angle combinations and mechanical efficiencies (as shown in Table 3) as well as variations due to external disturbances for each of the test cases.

### 2.3. Data Classification

Classification of all the data was necessary in order to train and learn from the parameter readings for new data.

The datasets were trained and classified using the k-NN algorithm. The k-NN classification method is an algorithm that stores all trained cases and classifies new cases based on a measure of similarity (Murphy, 2012). By this, the k-NN algorithm measures the distance between a new scenario against the already set scenarios from the generated data sets which would enable an approximation for classification for a new query. Distance measurement was calculated using the ‘Euclidean’ distance formula (Murphy, 2012) which is given by:

$$d_{st}^2 = (x_s - y_t)(x_s - y_t)' \quad (25)$$

The datasets generated from Section 2.2 were organised and trained for all the different tests conditions and cases for

classification using mean motor current values only. This was tested to evaluate the robustness and accuracy for new queries. New queries were selected for classification prediction using k-NN classifier. This was achieved using the built-in k-NN function in Matlab, the code for which can be found in the Appendix.

## 3. RESULTS AND DISCUSSION

This section is divided into two parts. The first shows the simulation results of the test cases described in Section 2.2. The second contains the analysis and classification of the trained data with new queries tested using k-NN classification algorithm.

### 3.1. Simulation Results

Simulations were run for three trapezoidal speed profiles – 500, 1500 and 3000 RPM as shown in Figure 8.

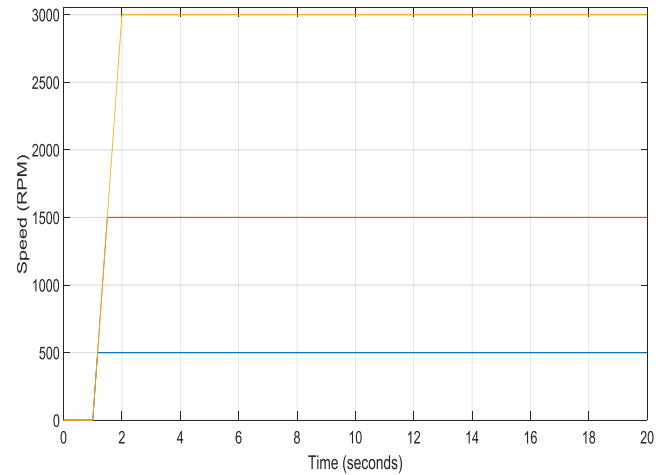


Figure 8. EMA Test Speed Profiles.

The corresponding 3-phase currents for 500 RPM is shown in Figure 9.

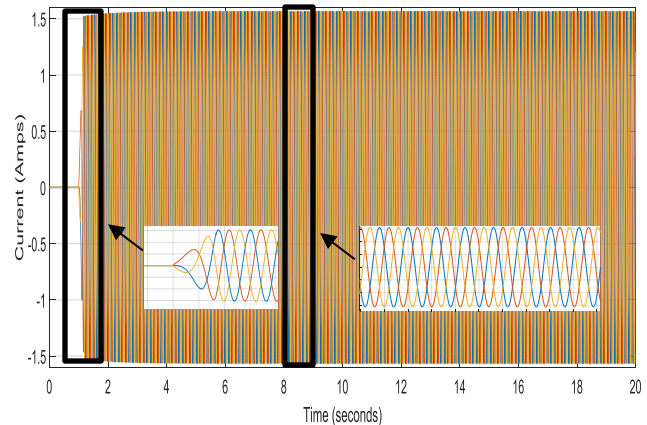


Figure 9. 3-Phase Currents (500 RPM).

As can be seen from the zoomed views in Figure 9, the motor starts to turn after 1 second, which corresponds to the initial ramp up as indicated in the speed profiles. After reaching steady state, the sinusoidal 3-phase alternating currents exhibit constant amplitudes as well as fixed width waveforms. The frequency was evaluated according to the peak to peak time period,  $t$  for a single phase current is 0.12 seconds:

$$f = \frac{1}{t} = \frac{1}{0.12} = 8.333\text{Hz}$$

The speed can then be calculated –

$$\omega = 2\pi f = 52.3599 \text{ rad/s}$$

Therefore,  $52.3599 \times \frac{30}{\pi} = 500 \text{ RPM}$  which corresponds correctly with the demand speed.

Park’s transform was performed to generate the equivalent  $I_q$  currents. These are shown for all speeds in Figure 10.

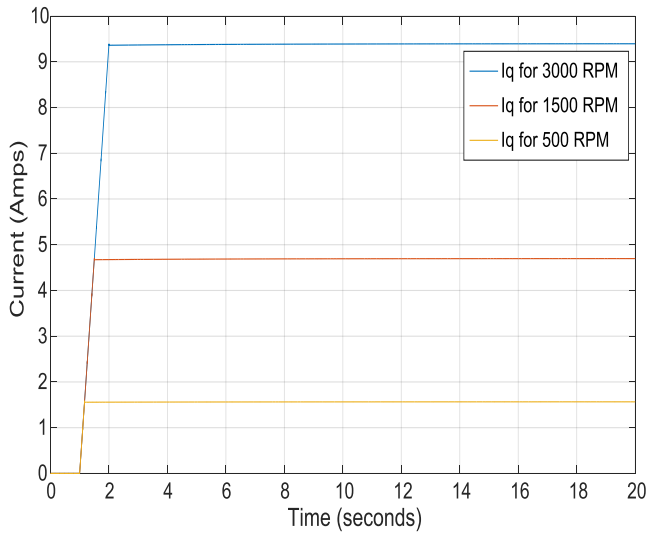


Figure 10.  $I_q$  Currents for All Speeds.

These simulations were run with measurements obtained without factoring in the effects of EMA ballscrew efficiency and other losses. Simulations were run for different contact angles and mechanical efficiencies added to evaluate the effect of  $I_q$  currents. Results are shown for Healthy, Degrading and Faulty conditions.

Healthy State

Firstly, the contact angles (between ball and nut, and ball and screw) were varied (as specified in Table 3). The resulting

maximum  $I_q$  currents are shown in Figure 11 for all speed demands with 80% mechanical system efficiency. (Each test case number corresponds to those listed in Table 4 where a summary of the results are shown.)

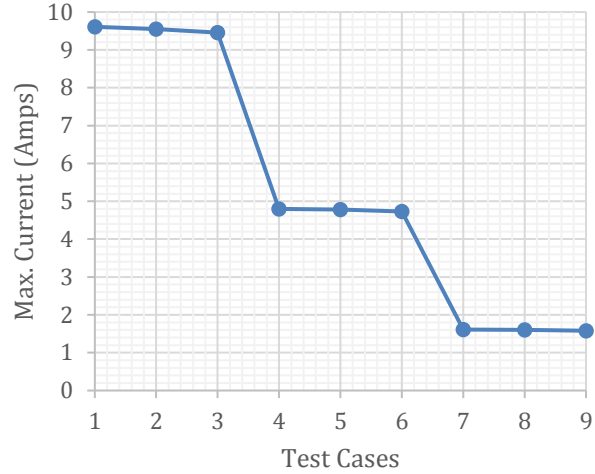


Figure 11. Maximum  $I_q$  Currents Under Varying Contact Angles for All Speeds (Healthy States).

Table 4. Maximum  $I_q$  Currents Under Varying Contact Angles for All Speeds (Healthy States).

Test Case	Demand Speed (RPM)	Contact Angle (deg)		Max. Current (Amps)
		BN	BS	
1	3000	40	40	9.61
2	3000	38	40	9.55
3	3000	38	38	9.46
4	1500	40	40	4.80
5	1500	38	40	4.78
6	1500	38	38	4.73
7	500	40	40	1.61
8	500	38	40	1.60
9	500	38	38	1.58

Figure 11 shows that more  $I_q$  current is drawn with increasing severity of B-N and B-S contact angles. However, the margins become increasingly smaller between the  $I_q$  currents (for respective contact angle cases) at lower speed demands. These cases were classified as being healthy although it could be challenging to diagnose against early stages of deterioration, especially when operating at low speeds.

The mechanical system efficiency was changed to 70% with resulting maximum  $I_q$  currents shown in Figure 12. Contact angles for B-N and B-S at 40 degrees are also presented

alongside the previous results with 80% efficiency. (Each test case number corresponds to those listed in Table 5 where a summary of the results are shown.)

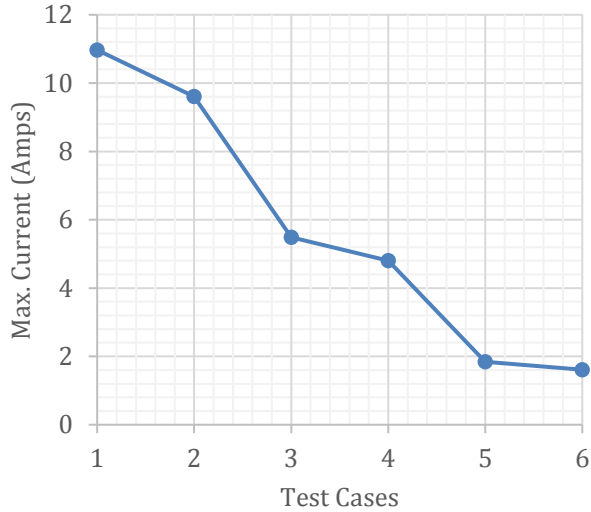


Figure 12. Maximum  $I_q$  Currents Under Varying Mechanical System Efficiencies for All Speeds (Healthy States).

Table 5. Maximum  $I_q$  Currents Under Varying Mechanical System Efficiencies for All Speeds (Healthy States).

Test Case	Demand Speed (RPM)	Mechanical System Efficiency (%)	Max. Current (Amps)
1	3000	70	10.97
2	3000	80	9.61
3	1500	70	5.49
4	1500	80	4.80
5	500	70	1.84
6	500	80	1.61

As can be seen from the  $I_q$  currents in Figure 12, the variation in mechanical system efficiency is more noticeable for each set of speed profiles.

Degrading State

Larger contact angle offsets were introduced (as specified in Table 3) to represent degrading cases to further analyse the effect on the  $I_q$  currents. A sample of these cases are presented in Figure 13. (Each test case number corresponds to those listed in Table 6 where a summary of the results are shown.)

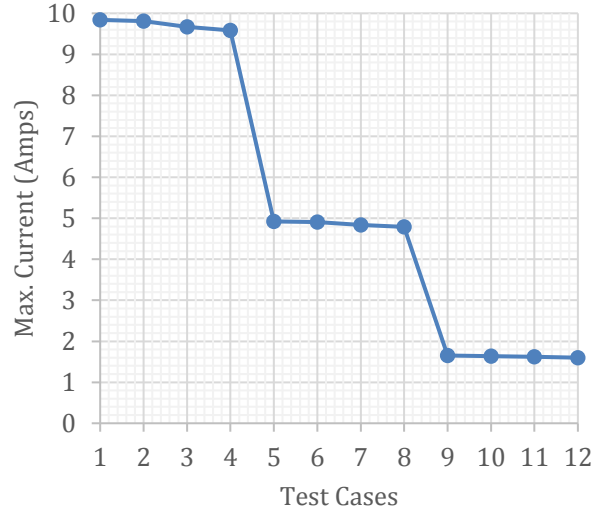


Figure 13. Maximum  $I_q$  Currents Under Varying Contact Angles for All Speed Profiles (Degrading States).

Table 6. Maximum  $I_q$  Currents Under Varying Contact Angles for All Speeds (Degrading States),

Test Case	Demand Speed (RPM)	Contact Angle (deg)		Max. Current (Amps)
		BN	BS	
1	3000	35	43	9.84
2	3000	43	43	9.81
3	3000	35	35	9.67
4	3000	43	38	9.58
5	1500	35	43	4.92
6	1500	43	43	4.91
7	1500	35	35	4.84
8	1500	43	38	4.79
9	500	35	43	1.65
10	500	43	43	1.64
11	500	35	35	1.62
12	500	43	38	1.60

Figure 13 shows the progressive nature of the ballscrew degradation where  $I_q$  currents are increasing with severity of contact angle offsets.

Variations in mechanical system efficiencies (for degrading conditions) were introduced and compared with a couple of examples of contact angle offsets. Table 7 shows the results of this where simulations were run at 3000 RPM command speed.

Table 7. Maximum  $I_q$  Currents Under Varying Mechanical System Efficiencies at 3000 RPM (Degrading States).

Test Case	Contact Angle (deg)		Mechanical System Efficiency (%)	Max. Current (Amps)
	BN	BS		
1	35	43	35	22.48
2	43	38	35	21.89
3	35	43	55	14.31
4	43	38	55	13.93
5	35	43	70	11.24
6	43	38	70	10.94

Significantly higher current is drawn with reducing mechanical system efficiencies. Not only is this indicative of a severely degraded system, the risk of overcurrent becomes more probable (peak current of the PMSM rated at 28.7 A as specified in Table 1).

Faulty State

Lower values of mechanical system efficiencies were modelled to represent faulted states of the EMA. The results of which are shown in Figure 14. (Each test case number corresponds to those listed in Table 8 where a summary of the results are shown.)

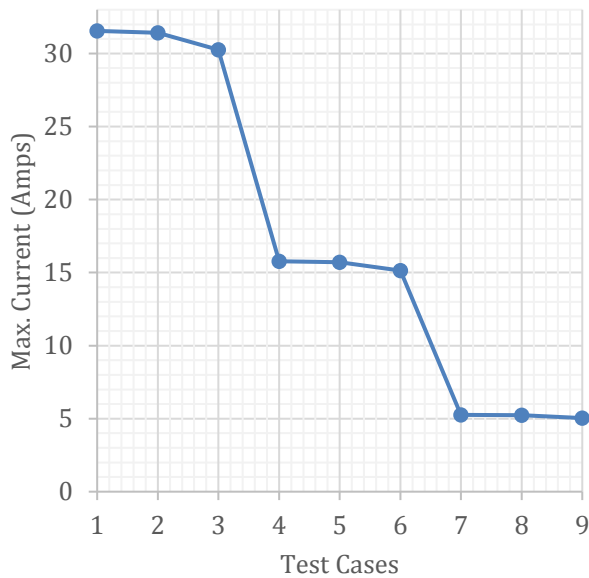


Figure 14. Maximum  $I_q$  Currents Under Varying Contact Angles for All Speeds with 25% Efficiency (Faulty States).

Table 8. Maximum  $I_q$  Currents Under Varying Contact Angles for All Speeds (Faulty) States).

Test Case	Demand Speed (RPM)	Contact Angle (deg)		Max. Current (Amps)
		BN	BS	
1	3000	35	35	31.55
2	3000	43	43	31.41
3	3000	38	38	30.27
4	1500	35	35	15.77
5	1500	43	43	15.71
6	1500	38	38	15.14
7	500	35	35	5.26
8	500	43	43	5.23
9	500	38	38	5.04

More specifically, the onset of ballscrew jamming was modelled by reducing the relative velocities between the ball and nut, and ball and screw. Table 9 shows the resulting maximum currents of such scenarios with simulations run at 3000 RPM demand speed.

Table 9. Maximum  $I_q$  Currents for Reducing Relative Velocities Between Ball-Nut and Ball-Screw.

Test Case	Conditions	Max. Current (Amps)
1	Relative velocities close to 0 in BN and BS	61.40
2	Relative velocities close to 0 in BS	52.68
3	Relative velocities close to 0 in BN	45.98

Table 9 shows that significantly more  $I_q$  currents are drawn when relative velocities (between B-N and B-S) are set close to zero. More  $I_q$  current is drawn for ball-screw interaction especially as this is the most contentious area of friction in a ballscrew (Vahid-Araghi and Golnaraghi, 2011).

Given the simulated data presented so far, further challenges become apparent which may lead to a misclassification of a health state. This can arise from data analysis of motor current signals where information relating to loads, operating speeds and quantification of system efficiency are unknown.

A misclassification can occur during an external disturbance such as gust or aeroloads.

Table 10. Example Misclassification Between Healthy and Degrading  $I_q$  Currents at 500 RPM.

Test Case	Mechanical System Efficiency (%)	External Load	Max. Current (Amps)	Health State
1	70	Yes	2.20	Healthy
2	65	No	1.95	Degrading

Table 10 shows an example of where, for the same demand speed, a misclassification can occur where the healthy signal experiences a higher  $I_q$  current than the degrading one due to external load disturbances.

**3.2. Data Classification**

A total of 667  $I_q$  current datasets were generated with each set processed to obtain mean current values (from steady state ~ 2 to 20 seconds cycle time) for training towards data classification.

The datasets were ‘supervised’ as the response to each set of variables are known i.e. Healthy, Degrading or Faulty. A sample set of mean  $I_q$  currents at 3000 RPM were plotted against their respective health state. The results are shown in Figure 15.

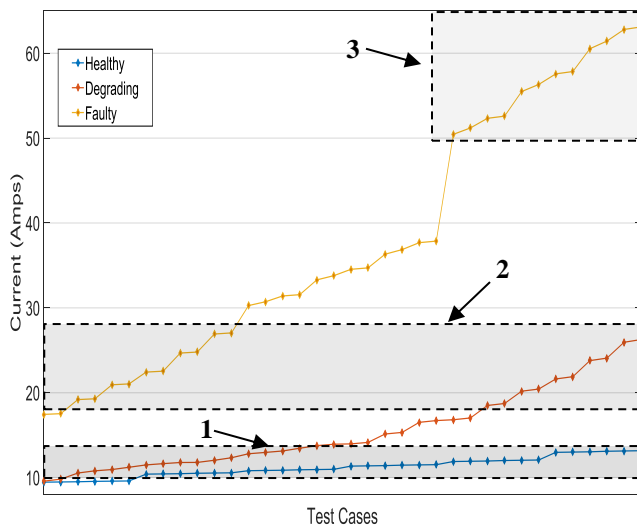


Figure 15. Sample Mean  $I_q$  Currents at 3000 RPM.

Here it can be seen that the risk of misclassification is much higher between healthy and degrading datasets (as can be seen from the region labelled 1) due to the overlap in observations. False results are also possible for data generated in the lower bounds of the faulty data and higher

bounds of the degrading data where the observations are overlapping (as can be seen from the region labelled 2). Despite the possibility of a misclassification, the actual health state of the EMA can be distinguishable outside regions 1 and 2. In particular, the onset of jamming can be predictable with such cases highlighted as shown in the region labelled 3.

In the context of aircraft maintenance of such systems, motor current and speed may be the only parameters available for diagnosis and fault detection during scheduled checks (Isturiz et al. 2012). Therefore, all mean  $I_q$  currents and speeds were classified and plotted against their respective health state. The trained data is displayed in the scatter plot in Figure 16.

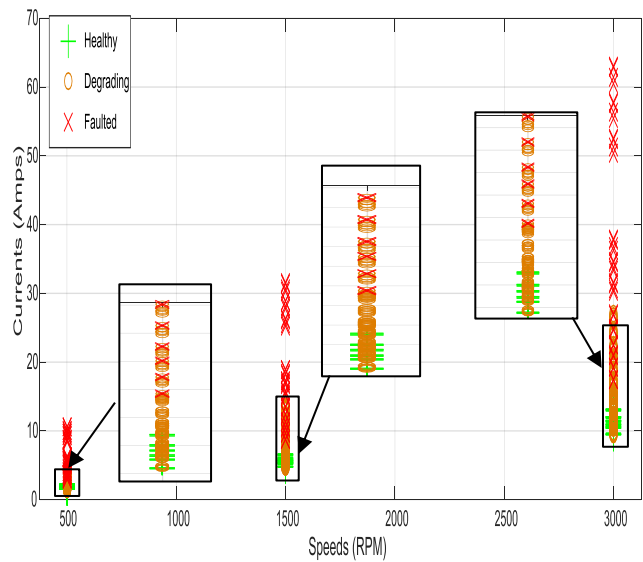


Figure 16. Classification of Data Based on  $I_q$  Currents and Speed.

As can be seen from Figure 16, false results are apparent as highlighted in the regions shown in the close ups.

A corresponding Confusion Matrix (Figure 17) was generated after training the data using k-NN classification algorithm to show the classification accuracy of these datasets given the conditions.

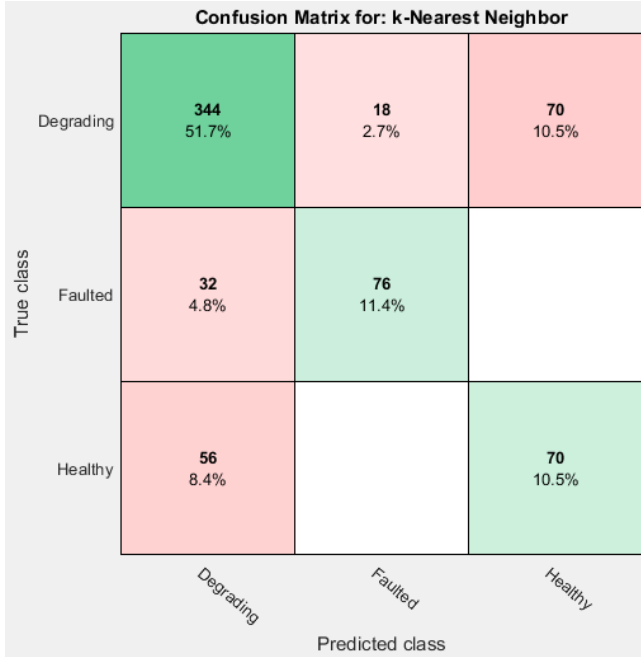


Figure 17. Confusion Matrix for Classifications with Knowledge of  $I_q$  Currents and Demand Speeds.

An overall classification accuracy of 73.6% was obtained. The red squares highlight instances of classification uncertainty from the simulated datasets. As can be seen, false results are most prevalent in cases where there is misclassification in data between Healthy and Degrading, and Degrading and Faulty states. It can also be seen that there are no misclassifications between Healthy and Faulted states.

The final step was to predict a classification (health state) based on the k-NN classifier for a new query. The queries to be evaluated were mainly based on situations where the data lies within a region of uncertainty of the trained classification. The queries to be tested are listed in Table 11.

Table 11. Queries to be Tested.

Query	Demand Speed (RPM)	$I_q$ current (Amps)
1	500	2.1
2	500	2.8
3	500	4.2
4	1500	5.1
5	1500	12.3
6	1500	12.7
7	3000	10.1
8	3000	23
9	1000	10
10	1850	21
11	2600	9

The first set of predictions were generated based on a k-NN classifier with a neighbourhood size of 1. The results of this are presented in Table 12.

Table 12. Predicted Classifications Using 1 NN.

Query	Demand Speed (RPM)	$I_q$ current (Amps)	Predicted Classification (NN = 1)
1	500	2.1	Degrading
2	500	2.8	Degrading
3	500	4.2	Faulted
4	1500	5.1	Healthy
5	1500	12.3	Faulted
6	1500	12.7	Degrading
7	3000	10.1	Degrading
8	3000	23	Faulted
9	1000	10	Degrading
10	1850	21	Faulted
11	2600	9	Healthy

A classifier can be more robust with more neighbours (Murphy, 2012) so a new set of predictions was generated for the same queries with increasing neighbourhood size. The results of this are shown in Table 13. Classifications highlighted in bold indicate a change in classification through each change in neighbourhood size value.

Table 13. Predicted Classifications Using Different NN Values.

Query	Predicted Classification				
	NN=1	NN=2	NN=3	NN=5	NN=10
1	Degrading	Degrading	Degrading	Degrading	Degrading
2	Degrading	Degrading	Degrading	Degrading	Degrading
3	Faulted	<b>Degrading</b>	<b>Faulted</b>	<b>Degrading</b>	Degrading
4	Healthy	Healthy	Healthy	Healthy	Healthy
5	Faulted	<b>Degrading</b>	Degrading	Degrading	Degrading
6	Degrading	Degrading	Degrading	Degrading	Degrading
7	Degrading	Degrading	Degrading	<b>Healthy</b>	<b>Degrading</b>
8	Faulted	<b>Degrading</b>	<b>Faulted</b>	<b>Degrading</b>	Degrading
9	Degrading	Degrading	<b>Faulted</b>	<b>Degrading</b>	Degrading
10	Faulted	Faulted	Faulted	Faulted	Faulted
11	Healthy	Healthy	Healthy	Healthy	Healthy

As can be deduced from Table 13, some queries exhibited consistency in terms of predicted classification result i.e. queries 1, 2, 4, 6, 10 and 11.

Inconsistency in predicted classification was evident for queries 3 and 8 in particular where ascertaining the true state of health was difficult given the variation in classification of the nearest respective neighbours. Due to the uncertainty of these queries, such classifications can be deemed inconclusive as they can give rise to false predictions.

**4. CONCLUSION**

Simulated data were generated from a detailed Matlab/Simulink EMA model and used for data classification using the k-NN algorithm. The EMA was modelled for speed and current control with the PMSM modelled using dq axis transform theory, which enabled analysis using Iq currents. The Stribeck model was included as a means to evaluate friction at a local level of the ballscrew as a function of relative velocities between the ball and nut, and the ball and screw.

The EMA model was able to detect changes to the ballscrew contact angles and geometry as well as variation in mechanical system efficiencies using Iq currents. The risk of misclassification was greater when simulations were run with external load disturbances added in. This can make it difficult to detect variations in contact geometry and efficiencies.

A total of 667 datasets were generated containing mean Iq currents for all the different combinations of ballscrew contact angles, mechanical system efficiencies and demand speeds. The data was trained and classified using the k-NN algorithm. A classification accuracy of 73.6% was obtained using knowledge of Iq currents and demand speeds alone.

The model could be improved by considering a tribology-based approach to the friction analysis by evaluating contact pressures between the contact zones in the ballscrew. This can be viewed as a follow-on to the detailed kinematic analysis and a validation step to the velocity dependent friction model. It is also suggested that new queries be predicted from real-time data as a means to further assess the performance of the k-NN classifier presented.

It is proposed that the approach can be utilised in conjunction with a real application or test stand data. By this, a hybrid approach to diagnostics could be satisfied by capturing any discrepancy between model based results and actual data, which can also help to isolate faults within the EMA drivetrain.

**ACKNOWLEDGEMENT**

This work was supported by the Systems Centre and the EPSRC funded Industrial Doctorate Centre in Systems (Grant EP/G037353/1) and Stirling Dynamics.

**REFERENCES**

Balaban, E., Saxena, A., Bansal, P., Goebel, K., Curran, S., & Stoelting, P. (2009). A Diagnostic Approach for Electromechanical Actuators in Aerospace Systems.

Balaban, E., Saxena, A., Goebel, K., Byington, C., Watson, M., Bharadwaj, S., and Smith, M. (2009). Experimental Data Collection and Modelling for Nominal and Fault Conditions on Electro-mechanical Actuators. *PHM*.

Balaban, E., Saxena, A., Narasimhan, S., Roychoudhury, I., and Goebel, K. (2011). Experimental Validation of

- a Prognostic Health Management System for Electro-Mechanical Actuators. *American Institute of Aeronautics and Astronautics*.
- Bennett, J., Mecrow, B., Atkinson, D., and Atkinson, G. (2010). Safety-critical design of electromechanical actuation systems in commercial aircraft. *IET Electric Power Applications*, 37-47.
- Bodden, D. S., Clements, S., Schley, B., and Jenney, G. (2007). Seeded Failure Testing and Analysis of an Electromechanical Actuator. *Aerospace Conference IEEE*, 1-8.
- Boeing. (1994). *757 Operations Manual*. Seattle: The Boeing Company.
- Bowden, F., and Tabor, D. (1950). *The Friction and Lubrication of Solids*. Oxford: Oxford University Press.
- Donald, S., Garg, S., Hunter, G., Guo, T.-H., and Semega, K. (2004). *Sensor Needs for Control and Health Management of Intelligent Aircraft Engines*. NASA Technical Paper.
- Hoffman, A., Hansen, I., Beach, R., Plencner, R., Dengler, R., Jefferies, K., and Frye, R. (1985). *Advanced Secondary Power System for Transport Aircraft*. NASA Technical Paper.
- Ismail, M., Balaban, E., and Spangenberg, H. (2016). Fault Detection and Classification for Flight Control Electromechanical Actuators. *Aerospace Conference. IEEE*.
- Isturiz, A., Vinals, J., Manuel, A., and Aitzol, I. (2012). Health Monitoring Strategy for Electromechanical Actuator Systems and Components, Screw Backlash and Fatigue Estimation. *Recent Advances in Aerospace Actuation Systems and Components*.
- Jiang, H., Song, X., Xu, X., Tang, W., Zhang, C., and Han, Y. (2010). Multibody dynamics simulation of Balls impact-contact mechanics in Ball Screw Mechanism. *2010 International Conference on Electrical and Control Engineering* (pp. 1320-1323). IEEE.
- Lee, W., Lee, J., Hong, M., Nam, S., Jeon, Y., and Lee, M. (2015). Failure Diagnosis System for a Ball-Screw by Using Vibration Signals. *Hindawi Shock and Vibration*.
- McNier, T. (2016). *Specifying, Selecting and Applying Linear Ball Screw Drives*. Thomson.
- Murphy, K. (2012). *Machine Learning, A Probabilistic Perspective*. The MIT Press.
- Ninomiya, M., and Miyaguchi, K. (1998). Recent Technical Trends in Ball Screws. *NSK Technical Journal: Motion Control*, 1-3.
- Park, R. H. (1929). Two Reaction Theory of Synchronous Machines. *AIEE Transactions* 48, 716-730.
- Song, X., Jian, L., Zhao-tan, W., Xian-yin, L., and Bao-min, L. (2005). Research and Development of Test System of Combination Property of High-Speed Ball Screw Unit. *Tool Engineering*, 34-36.
- Vahid-Araghi, O., and Golnaraghi, F. (2011). *Friction-Induced Vibration in Lead Screw Drives*. Springer.
- Vas, P. (1996). *Electrical Machines and Drives: A Space-Vector Theory Approach*. Oxford.
- Wei, C., and Lin, J. (2004). Kinematic Analysis of the Ball Screw Mechanism Considering Variable Contact Angles and Elastic Deformations. *ASME Journal of Mechanical Design*, 717-733.
- Xu, S., Yao, Z., Sun, Y., and Shen, H. (2014). Load Distribution of Ball Screw With Consideration of Contact Angle Variation and Geometry Errors. *International Mechanical Engineering Congress and Exposition*. ASME.

#### BIOGRAPHIES

**Yameen Monsur Hussain** received a BEng (Hons) in Aviation Engineering from Brunel University, London in 2010 and MSc in Fluid Power Systems from the University of Bath in 2011. He is currently an Engineering Doctorate (EngD) student at the University of Bristol studying Health Monitoring of Electrical Actuation Systems in collaboration with Stirling Dynamics Ltd. His current research interests are prognostics and health management techniques, reliability, electromechanical actuation, tribology and optimisation of maintenance scheduling.

**Stephen G Burrow** received the MEng and PhD degrees in electrical engineering from the University of Bristol in 1998 and 2002, respectively. He is currently a Reader in the Department of Aerospace Engineering, University of Bristol. His current research encompasses power electronics, machines and energy harvesting, and environmental sensing.

**Leigh Henson** received a BEng (Hons) degree in Mechanical Engineering from the University of Huddersfield in 2002 including a twelve month industrial placement at AgustaWestland Helicopters (now Leonardo). Awarded Chartered Engineer (CEng) status as a member of the Institute of Mechanical Engineers (IMechE) in 2006 after four years post graduate experience in the civil aerospace industry with Airbus. Working for Stirling Dynamics has built extensive experience in Landing Gear Systems covering research and technology, new aircraft/equipment

development and qualification including: requirements capture, V&V process, first flight, flight test, certification, entry into service (EIS) and continuous product development (CPD).

**Patrick Keogh** received degrees from the universities of Nottingham and Manchester. He was a Research Technologist at the Engineering Research Centre, GEC Alstom (now Alstom). In 1990, he joined the Department of Mechanical Engineering, University of Bath, Bath, U.K. His current research interests include rotor dynamics, magnetic bearing systems, active vibration control, modern optimal control for multivariable systems, contact dynamics, and associated thermal behaviour of bearings.

#### APPENDIX

Matlab code to test new queries using the k-NN classifier.

```
load simulateddata
X = meas; %all motor current and speed
data
Y = responses %corresponding state of
health of each simulation
mdl = ClassificationKNN.fit(X,Y); %k-NN
classification
mdl.NumNeighbours = 1; %set number of
nearest neighbours, default value is 1
% Predict the classification for a new
query
query1 = [500 2.2]; %example query for
500 RPM and 2.2A
query1Class= predict(mdl,query1); %class
prediction
```